INTERNATIONAL JOURNAL FOR NUMERICAL METHODS IN FLUIDS, VOL. 10, 753–769 (1990)

A MOVING FINITE ELEMENT METHOD FOR THE POPULATION BALANCE EQUATION

T. H. TSANG AND A. RAO

Department of Chemical Engineering, University of Kentucky, Lexington, Kentucky 40506-0046, U.S.A.

SUMMARY

A moving finite element algorithm has been compared against the upwind-differencing and Smolarkiewicz methods for the population balance equation of multicomponent particle growth processes. Analytical solutions and an error function have been used to test the numerical methods. The moving finite elements technique is much more accurate than other methods for a wide range of parameters. Since this method uses moving grids, it is able to model very narrow particle size distributions. It is also shown that the method can be extended to solve condensational growth problems which include particle curvature and non-continuum mass transfer effects.

KEY WORDS Moving finite element method Population balance equation Particle growth First-order hyperbolic partial differential equation

INTRODUCTION

Continuous transport equations together with constitutive models of material behaviour are commonly used in engineering for fluid flows, heat and mass transfer equations apply to materials of continuous phase. However, dispersed multiphase systems abound in nature and in numerous engineering processes. Clouds in the atmosphere, crystals in crystallizers, precipitates and aerosols in colloidal systems, liquid droplets in liquid–liquid extraction systems, fluidized particles, coarsening particles in alloys, and microbial cell populations are common examples, to name just a few. Depending on each individual process, the particulate phase may be a pure substance or a multicomponent mixture. The pupulations balance equations is often required to model the formation, growth and shrinkage of the particulate phase. The dynamic behaviour of the particulates may be described by the number density function, which depends on properties space (e.g. particle size and composition) and physical space ((x, y, z) co-ordinates in spatially inhomogeneous systems). A review on the use of the population balance equation in numerous dispersed multiphase systems can be found in Reference 1.

In this work we are interested in the dynamic behaviour of the particulate phase and we only consider spatially homogeneous systems. Extension to spatially inhomogeneous systems can be achieved through the operator-splitting scheme as shown by Tsang and Brock.[2] Among numerous dispersed multiphase systems, we further restrict ourselves to aerosol systems. However, the numerical methods discussed below can be used for other particulate processes. Particles grow by coagulation and by condensation of the transferable species from the continuous phase to the particulate phase. When particles grow by condensation, the size distribution approaches monodispersity and the number density function has extremely large gradients. Most numerical methods create either excessive numerical diffusion or severe spurious oscillations. The objective

0271–2091/90/070753–17$08.50

Received 22 August 1988
Revised 31 July 1989

of this work is to demonstrate that a moving finite element method can provide accurate numerical solutions to condensational growth of multicomponent particles.

PROBLEM STATEMENT

Subsequent to their appearance by homogeneous nucleation, particles grow by coagulation and condensation processes. If the coagulation process is much slower than the condensation process, coagulation can be neglected. Brock[3] showed that Brownian coagulation is insignificant for particles with mean diameter greater than 0·1 μm.

For multicomponent systems the population balance equation of particle growth by condensation is

$$\frac{\partial n}{\partial t}+\sum_{i=1}^{N}\frac{\partial}{\partial m_i}(\psi i n)=0. \tag{1}$$

Here $\int\cdots\int n(m_1, m_2, \ldots, m_N, t)\mathrm{d}m_1\,\mathrm{d}m_2\ldots\mathrm{d}m_N$ is the number of particles with masses in the range of m_1 and $m_1+\mathrm{d}m_1$, m_2 and $m_2+\mathrm{d}m_2, \ldots, m_N$ and $m_N+\mathrm{d}m_N$, where N is he number of condensing species in the aerosol system. Multicomponent systems are commonly found in atmospheric aerosols and aerosols generated in chemical reacting systems. The latter is of particular interest because of its potential in the production of multicomponent fine particles of ceramic and semiconducting materials. Equation (1) finds common applications in crystallization, precipitation and particle growth processes in alloy and aerosol systems.

In equation (1), ψi is the particle growth rate for the ith component and m_i is the mass of the ith component in a particle. For a dilute vapour–gas mixture the growth rate can be expressed by the Maxwell equation[4]

$$\psi i=2\pi D_i d_\mathrm{p}(Ci_\infty-Ci_{r_\mathrm{p}}), \tag{2}$$

where D_i is the vapour diffusivity of the ith component, d_p is the particle diameter, which relates to the total mass of a particle through the liquid density, and Ci_∞ and Ci_{r_p} are the vapour concentration of the ith component in the gas phase and at the particle surface respectively. The vapour concentration at the particle surface is related to the vapour pressure P^0_{vi} of pure ith component through the generalized Kelvin equation

$$\ln\left(\frac{Ci_{r_\mathrm{p}}}{Ci_\mathrm{v}}\right)=\frac{4\gamma v_i}{d_\mathrm{p}RT}=Ke_i, \tag{3}$$

where Ci_v is the equilibrium concentration of the ith component over a planar surface of solution. $Ci_\mathrm{v}=P^0_{vi}x_i\bar{M}_i/RT$, where x_i and $\bar{M}_i$ are the mole fraction and molecular weight of the ith component respectively. R is the universal gas constant and T is the system temperature. In equation (3), γ is the surface tension of the multicomponent droplet, v_i is the particle molar volume of the ith component and Ke_i is the Kelvin number of the ith component. The generalized Kelvin equation (3) has been a subject of controversial debate in the past decade. However, the controversy was resolved recently by Mirabel and Reiss[5] and Wilemski.[6] They proved that equation (3) is the correct generalized Kelvin equation.

Equation (2), the Maxwell equation, is the result of steady state solution of a simple diffusion problem. It is valid for particles with relatively large diameter or small Knudsen number $Kn_i=2\lambda_i/d_\mathrm{p}$, where λ_i is the mean free path of the ith component. For particles with Kn_i of the order of unity, the continuum Fick's diffusion law no longer applies. For particles with very small diameter, i.e. $Kn_i\gg 1$, the kinetic theory of gases applies. In the transition regime where

$0{\cdot}1 \leqslant Kn_i \leqslant 10$, no complete transport theory exists.[7] To correct the particle growth process in the transition regime, the interpolation formula of Fuchs and Sutugin[8] is used. Recently, Ray *et al.*[9] showed that it fitted the experimental data quite satisfactorily. Thus equations (2) and (3), with the inclusion of Fuchs and Sutugin's interpolation formula $f(Kn_i)$, are modified to

$$\psi i = 2\pi D_i d_p Ci_v (S_i - e^{Ke_i}) f(Kn_i) \tag{4}$$

where $S_i = Ci_\infty / Ci_v$ is the saturation ratio of the ith component and

$$f(Kn_i) = \frac{1 + Kn_i}{1 + 1{\cdot}71 Kn_i + 1{\cdot}333 Kn_i^2}. \tag{5}$$

The initial and boundary conditions for equation (1) are

$$n(m_1, m_2, \ldots, m_N, 0) = n_0(m_1, m_2, \ldots, m_N), \tag{6}$$

$$n(m_i, t)|_{m_i \to \infty} = 0. \tag{7}$$

In equation (6), n_0 is the initial size distribution. Here we use a log-normal distribution for n_0, although other size distributions can be used. Equation (7) implies that there is no large particle in the population. In practice, instead of equation (7), other satisfactory approximations can be used, as will be discussed later.

Since the domain of interest in the particulate phase usually covers several orders of magnitude in particle diameter or about 10 orders of magnitude in particle mass, it is desirable to transform equation (1) into the following form (J-space transformation by Middleton and Brock[10]). For the sake of clarity we consider binary systems.

$$\frac{\partial f}{\partial \tau} + \sum_{i=1}^{2} \frac{\partial}{\partial Ji} (\overline{\psi i} f) = 0, \tag{8}$$

where $f(J1, J2) = \alpha^2 \pi_i m_i n(m_1, m_2)$, $m_i = m_{i0} e^{\alpha(Ji-1)}$, $\overline{\psi i} = \psi i / \alpha m_i$ and $\tau = t$; m_{i0} is the mass of the ith component in the smallest particle of the population and α is a scaling parameter. Here we use $\alpha = 1$, implying that 10 units of Ji value cover a decade of particle diameter. In the following we present a moving finite element method for equation (8).

A MOVING FINITE ELEMENT METHOD

Equation (8) applies to many particulate processes and is called the 'equation of continuity', seemingly because of its similarity with its counterpart in hydrodynamics. It is a first-order hyperbolic partial differential equation. Its numerical solution is a formidable job because most numerical methods suffer from either numerical diffusion or spurious oscillations. A high-order-accurate scheme such as the Galerkin finite element method is particularly susceptible to spurious oscillations since the size distribution narrows and approaches monodispersity during the particle growth process, thus creating extremely large values of $\partial f / \partial Ji$. Low-order-accurate schemes such as upwind differencing do not create spurious oscillations but have an intolerable amount of numerical diffusion. In general, numerical methods using fixed grid systems cannot resolve the problem of large gradients generated during the particle growth period. Therefore, for single-component particle growth problems, Tsang and Brock[11] have used a moving finite element method based on the algorithm by Varoglu and Finn.[12] In modelling the dynamic approach to monodispersity, only 80 grid points were used. The grid points move with the condensation rate or the characteristic velocity to extremely narrow size range to provide high

resolution. The dimensionless grid intervel corresponds to the use of a numerical method with a fixed grid system of approximately 2300 grid points per decade of particle diameter!

It should also be mentioned that the recent success of computational fluid dynamics is partially due to the use of mesh refinement, which can be achieved through mesh movement, mesh enriching or remeshing. Adaptive remeshing or enriching schemes are highly successful in modelling transport and shock problems.[13-15] In this work we extend Varoglu and Finn's one-dimensional moving finite element method to multidimensional problems. Derivation of the algorithm follows closely Varoglu and Finn's approach.

If $\hat{f}$ be an approximation to the solution $f(J1, J2, \tau)$. Then the vanishing of the weighted residual with respect to a continuous function $\phi(J1, J2, \tau)$ defined on

$$J1_{\min} \leqslant J1 \leqslant J1_{\max}, \quad J2_{\min} \leqslant J2 \leqslant J2_{\max}, \quad \tau_1 \leqslant \tau \leqslant \tau_2$$

can be expressed as

$$\int_{\tau_1}^{\tau_2} \int_{J1_{\min}}^{J1_{\max}} \int_{J2_{\min}}^{J2_{\max}} \left(\frac{\partial \hat{f}}{\partial \tau} + \frac{\partial}{\partial J1} (\overline{\psi 1} \hat{f}) + \frac{\partial}{\partial J2} (\overline{\psi 2} \hat{f}) \right) \phi(J1, J2, \tau) \mathrm{d}J1 \, \mathrm{d}J2 \, \mathrm{d}\tau = 0, \tag{9}$$

where τ_1 and τ_2 are the nth and $(n+1)$th time levels. Integrating parts we have

$$\int_{\tau_1}^{\tau_2} \int_{J1_{\min}}^{J1_{\max}} \int_{J2_{\min}}^{J2_{\max}} \left(-\hat{f} \frac{\partial \phi}{\partial \tau} - \overline{\psi 1} \hat{f} \frac{\partial \phi}{\partial J1} - \overline{\psi 2} \hat{f} \frac{\partial \phi}{\partial J2} \right) \mathrm{d}J1 \, \mathrm{d}J2 \, \mathrm{d}\tau + \int_{J1_{\min}}^{J1_{\max}} \int_{J2_{\min}}^{J2_{\max}} [\hat{f}\phi]_{\tau_1}^{\tau_2} \mathrm{d}J1 \, \mathrm{d}J2$$
$$- \int_{\tau_1}^{\tau_2} [(-\overline{\psi 1} \hat{f} \phi)_{J1} + (-\overline{\psi 2} \hat{f} \phi)_{J2}] \mathrm{d}\tau = 0. \tag{10}$$

The problem is solved step by step in time using space–time finite elements.

The distorted brick elements are transformed from the $J1$–$J2$–τ global co-ordinate system to an r–s–t local co-ordinate system such that the trasformed element is a cube ($-1 \leqslant r \leqslant 1$, $-1 \leqslant s \leqslant 1$, $-1 \leqslant t \leqslant 1$). The relationships for co-ordinate transformation are as follows:

$$Ji = \sum_{i=1}^{8} N_i Ji_{ij}, \tag{11}$$

$$\tau = \tfrac{1}{2} [(1-t)\tau_1 + (1+t)\tau_2], \tag{12}$$

where Ji is either $J1$ or $J2$, N_i denotes the shape functions and Ji_{ij} are the nodal values of Ji.

For an eight-node brick element the shape functions are

$$N_1 = \tfrac{1}{8}(1+r)(1-s)(1+t), \qquad N_2 = \tfrac{1}{8}(1+r)(1+s)(1+t),$$
$$N_3 = \tfrac{1}{8}(1-r)(1+s)(1+t), \qquad N_4 = \tfrac{1}{8}(1-r)(1-s)(1+t),$$
$$N_5 = \tfrac{1}{8}(1+r)(1-s)(1-t), \qquad N_6 = \tfrac{1}{8}(1+r)(1+s)(1-t),$$
$$N_7 = \tfrac{1}{8}(1-r)(1+s)(1-t), \qquad N_8 = \tfrac{1}{8}(1-r)(1-s)(1-t). \tag{13}$$

The relation between the differential variables is expressed as

$$\mathrm{d}J1 \, \mathrm{d}J2 \, \mathrm{d}\tau = \left| \frac{\partial(J1, J2, \tau)}{\partial(r, s, t)} \right| \mathrm{d}r \, \mathrm{d}s \, \mathrm{d}t = |J| \, \mathrm{d}r \, \mathrm{d}s \, \mathrm{d}t, \tag{14}$$

where $\partial(J1, J2, \tau)/\partial(r, s, t)$ is the Jacobian of the transformation. Evaluating this Jacobian rigorously results in very involved expressions and the coefficient matrix for binary compounds has nine diagonals. The problem was simplified at this step in order to reduce both computing

time and storage. This simplification reduces the final solution for binary systems to a pentadiagonal matrix without sacrificing much of the accuracy, as will be shown later. Similarly, the global element matrix for ternary systems can be reduced to a seven-diagonal matrix. The simplification was introduced by assuming that, in evaluating the Jacobian, an element in the $J1$–$J2$ plane was treated as a rectangle rather than a quadrilateral. This implies that $J1_{ij}=J1_{i,j+1}$ and $J2_{ij}=J2_{i+1,j}$. Therefore equation (1)) yields

$$J1=\tfrac{1}{4}[(1-s)(1+t)\,J1_{ij}^{n}+(1+s)(1+t)J1_{ij}^{n+1}+(1-s)(1-t)\,J1_{i+1,j}^{n}+(1+s)(1-t)\,J1_{i+1,j}^{n+1}], \quad (15)$$

$$J2=\tfrac{1}{4}[(1-s)(1+r)]\,J2_{ij}^{n}+(1+s)(1+r)\,J2_{ij}^{n+1}+(1-s)(1-r)\,J2_{i,j+1}^{n}+(1+s)(1-r)\,J2_{i,j+1}^{n+1}]. \quad (16)$$

The Jacobian now simplifies to

$$|J|=(k/32)\{[(1-s)\,J1_{ij}^{n}+(1+s)J1_{ij}^{n+1}-(1-s)\,J1_{i+1,j}^{n+1}-(1+s)\,J1_{i+1,j}^{n}][(1-s)\,J2_{ij}^{n}$$
$$+(1+s)\,J2_{ij}^{n+1}-(1-s)\,J2_{i,j+1}^{n+1}-(1+s)\,J2_{i,j+1}^{n}]\}, \quad (17)$$

where $k=\tau_2-\tau_1$ is the time step.

In the local co-ordinates the approximate solution over a typical element is a polynomial of the form

$$\hat{f}(r,s,t)=\sum_{i=1}^{8} N_i\hat{f}_{ij}. \quad (18)$$

The weighting function ϕ in equation (9) is uniquely determined by its values at all the nodes P_{ij}^{n} $(i=1,2,\ldots,I, j=1,2,\ldots,J)$ and is linear along the sides of the finite elements. For each node at a time level n it is define as

$$\phi^{(k1)}(P_{ij}^{n})=\begin{cases}1, & k=i \text{ and } l=j,\\ 0, & \text{otherwise.}\end{cases} \quad (19)$$

Replacing $\phi(J1,J2,\tau)$ by $\phi^{(ij)}(i=2,3,\ldots,I\text{-}1,\ j=2,3,\ldots,J\text{-}1)$, $(I\text{-}2)(J\text{-}2)$ equations in the unknowns f_{ij}^{n+1} are obtained from equation (10) as follows:

$$\sum_{k=2}^{I-1}\sum_{l=2}^{J-1}\iiint_{S_{kl}^{n}}\left(-\hat{f}\frac{\partial\phi^{(ij)}}{\partial\tau}-\overline{\psi 1}\hat{f}\frac{\partial\phi^{(ij)}}{\partial J1}-\overline{\psi 2}\hat{f}\frac{\partial\phi^{(ij)}}{\partial J2}\right)dJ1\,dJ2\,d\tau$$
$$+\int_{J1_{\min}}^{J1_{\max}}\int_{J2_{\min}}^{J2_{\max}}[\hat{f}\phi^{(ij)}]_{\tau_1}^{\tau_2}\,dJ1\,dJ2$$
$$-\int_{\theta^{n}}^{\theta^{n+1}}[(-\overline{\psi 1}\hat{f}\phi^{(ij)})_{J1_{\min}}^{J1_{\max}}+(-\overline{\psi 2}\hat{f}\phi^{(ij)})_{J2_{\min}}^{J2_{\max}}]d\tau=0, \quad i=2,3,\ldots I\text{-}1, \quad j=2,3,\ldots,J\text{-}1 \quad (20)$$

where subscripts min and max correspond to the minimum and maximum value respectively.

The integral is approximated by

$$\iiint_{\hat{S}}\hat{\Psi}(r,s,t)\,dr\,ds\,dt=\tfrac{1}{8}\sum_{s=1}^{8}\hat{\Psi}(\hat{P}_s), \quad (21)$$

where $\{\hat{P}_s\}_{s=1}^{8}$ denotes the eight nodes of the brick element $\hat{S}$ and $\hat{\Psi}$ is an arbitrary function defined on $\hat{S}$.

Using the Jacobian, evaluating each integral term in equation (20) and summing over each element without showing lengthy intermediate steps, we have the final result

$$\begin{aligned}
&\tfrac{1}{2}f^{n+1}_{i+1,j}\{[k\overline{\psi 1}^{n+1}_{i+1,j}-(J1^{n+1}_{i+1,j}-J1^{n}_{i+1,j})](J2^{n+1}_{i+1,j+1}-J2^{n+1}_{i+1,j-1})\}\\
&\quad+\tfrac{1}{2}f^{n+1}_{i-1,j}\{[-k\overline{\psi 1}^{n+1}_{i-1,j}+(J1^{n+1}_{i-1,j}-J1^{n}_{i-1,j})](J2^{n+1}_{i-1,j+1}-J2^{n+1}_{i-1,j-1})\}\\
&\quad+\tfrac{1}{2}f^{n+1}_{i,j+1}\{[k\overline{\psi 2}^{n+1}_{i,j+1}-(J2^{n+1}_{i,j+1}-J2^{n}_{i,j+1})](J1^{n+1}_{i+1,j+1}-J1^{n+1}_{i-1,j+1})\}\\
&\quad+\tfrac{1}{2}f^{n+1}_{i,j-1}\{[-k\overline{\psi 2}^{n+1}_{i,j-1}+(J2^{n+1}_{i,j-1}-J2^{n}_{i,j-1})](J1^{n+1}_{i+1,j-1}-J1^{n+1}_{i-1,j-1})\}\\
&\quad+2f^{n+1}_{ij}[(J1^{n+1}_{i+1,j}-J1^{n+1}_{i-1,j})(J2^{n+1}_{i,j+1}-J2^{n+1}_{i,j-1})]\\
&=2f^{n}_{ij}[(J1^{n}_{i+1,j}-J1^{n}_{i-1,j})(J2^{n}_{i,j+1}-J2^{n}_{i,j-1})]\\
&\quad+\tfrac{1}{2}f^{n}_{i,j+1}[(J2^{n+1}_{i,j+1}-J2^{n}_{i,j+1})(J1^{n}_{i-1,j+1}-J1^{n}_{i+1,j+1})]\\
&\quad-\tfrac{1}{2}f^{n}_{i,j-1}[(J2^{n+1}_{i,j-1}-J2^{n}_{i,j-1})(J1^{n}_{i-1,j-1}-J1^{n}_{i+1,j-1})]\\
&\quad-\tfrac{1}{2}f^{n}_{i,j+1}[(k\overline{\psi 2}^{n}_{i,j+1})(J1^{n}_{i-1,j+1}-J1^{n}_{i+1,j+1})]\\
&\quad+\tfrac{1}{2}f^{n}_{i,j-1}[(k\overline{\psi 2}^{n}_{i,j-1})(J1^{n}_{i-1,j-1}-J1^{n}_{i+1,j-1})].
\end{aligned}\tag{22}$$

The above equation represents extensions of the one-dimensional problems formulated by Varoglu and Finn[12] and more recently by Blom *et al.*[16] In order to obtain a numerical solution for f^{n+1} in equation (22), it is necessary to calculate the location of grid points at the $n+1$ unknown time level (e.g. $J1^{n+1}_{i+1,j}$, $J2^{n+1}_{i+1,j+1}$, etc.). Two equations are required

$$\begin{aligned}
J1^{n+1}_{ij}&=J1^{n}_{ij}+k\overline{\psi 1}^{n}_{ij},\\
m_2^{n+1}&=\frac{\psi 2}{\psi 1}m_1^{n+1}-\frac{\psi 2}{\psi 1}m_1^{n}+m_2^{n},
\end{aligned}\tag{23}$$

where $\psi 1$ and $\psi 2$ are evaluated at the known time level. $J2^{n+1}$ can be found from m_2^{n+1} by using the definition of the J-space transformation. Alternatively, the first equation may also be ued for $J2^{n+1}$ (in this case it becomes a completely Lagrangian approach for mesh movement). For simple forms of ψi there are no significant differences in the numerical results for these two approaches. For case 3 (to be discussed later), both approaches to calculating $J2^{n+1}$ will give stable numerical results. However, for realistic growth rates such as equations (4) and (5), calculations of m_2^{n+1} according to equation (23) give stable and accurate results for case 4, whereas the completely Lagrangian approach suffers severe spurious oscillations near the regions of extremely large gradients. For compounds of different condensation rates the second equation implies that the grid point move in the $J2$-direction in proportion to their condensation rate. Component 1 is chosen to be the least volatile compound (e.g. smallest condensation rate) in the system equations (22) and (23). Additional terms arising from nucleation, sedimentation and coagulation can be treated by a time-splitting scheme, as is done successfully by Tsang and Brock.[2]

Equation (7) represents the formal boundary condition of equation (1). However, the numerical solution of equation (22) requires the boundary conditions for f_{1j}, f_{i1}, f_{iJ} and f_{Ij}. We find that accurate results can be obtained by using $f_{iJ}=f_{i,J-1}$ and $f_{Ij}=f_{I-1,j}$. Similarly, we assume that f_{1j} and f_{i1} are equal to their initial values. These procedures are admittedly ad hoc in nature, but it should be mentioned that only the f-values within the first three rows or columns of the boundary are slightly affected. Furthermore, these f-values are usually many orders of magnitude smaller than those around the mean diameter. For general transport problems in fluid flow, heat and mass transfer, special finite elements at the boundary must be devised.[12]

RESULTS AND DISCUSSION

In order to validate the moving finite element method described in the previous section, we use a simplified form of equation (2) for which we can obtain an analytical solution. The assumptions being used are as follows: (a) no Kelvin (curvature) effect, (b) negligible non-continuum effect on mass transfer, (c) ideal solution behaviour, (d) dilute vapour–gas mixture, (e) ideal mixing inside the liquid drops and (f) constant condensing vapour concentrations. Thus equation (2) can be written as $\psi i = a_i \left(\sum_j m_j \right)^{1/3} - d_i \left(\sum_j m_j \right)^{1/3} r_i$ is a function of the mole fraction of the ith component, a_i and d_i being some numerical constants. A further simplification results when the second term is neglected, implying that the condensation rate is at the upper limit of the growth law. Tsang and Rao[17] compared the method of moments, upwind differencing and a moving finite element method for single-component growth problems and found that if a numerical method can model a fast growth process it will be able to model slower processes. However, the reverse is not true. This allows us to write ψi as

$$\psi i = a_i \left(\sum_j m_j \right)^{1/3}. \tag{24}$$

For binary systems the analytical solution is

$$n(m_1, m_2, \ldots, t) = n_0 \frac{\left[\left(\sum_i m_{i0} \right)^{2/3} - \frac{2}{3} \sum_i (a_i) t \right]^{1/2}}{\left(\sum_i m_{i0} \right)^{1/3}}. \tag{25}$$

The initial size distribution is a log–normal size distribution of the form

$$n_0(m_1, m_2) = \frac{M_0}{m_1 m_2 [\sqrt{(2\pi)}(\ln \sigma)]^2} \exp\left(- \sum_i \frac{(\ln m_i - \ln \bar{m}_i)^2}{2(\ln \sigma)^2} \right), \tag{26}$$

where M_0 is the total particle number concentration (cm^{-3}), σ is the standard deviation of the distribution, m_i are the component masses and $\bar{m}_i$ is the mass of the ith component in the particle having the mean diameter in the distribution.

The availability of analytical solutions greatly facilitates the assessment of numerical methods. We introduce the following error function as a measure of accuracy of numerical solutions:

$$\| E \| = \frac{\sqrt{\left(\sum_i [(f_{\text{analyt}} - f_{\text{numeric}}) \Delta J1_i \Delta J2_i]^2 \right)}}{\sum_i f_{\text{analyt}} \Delta J1_i \Delta J2_i}, \tag{27}$$

where the f-values are the average values in the ith element. The summation was carried out over each element in the $J1$–$J2$ space. $f \Delta J1_i \Delta J2_i$ represents the number concentration of the ith element. The denominator is used as a normalizing factor since the total number concentration of aerosol particles may range from 10^3 to 10^{12} cm^{-3}.

In the following we first present three case studies for which we can compare our numerical results (MULFEMM) with analytical solutions. Numerical solutions from the positive definite methods of Smolarkiewicz[18] and upwind differencing are also included in this study because of the fact that upwind differencing and its variants are currently used in large-scale simulations of aerosol growth.[17,19,20] Explicit time differencing and a time-splitting scheme are used for the

upwind-differencing method and the Smolarkiewicz method. For the latter method we did not include a correction for the divergent velocity field and we used two corrective iterations since more iterations only led to slightly improved numerical solutions with a significant increase in computing time.

Case 1. Slow growth process with equal condensation rates

The initial size distribution is characterized by the initial number concentration of $1{\cdot}67 \times 10^6\ \mathrm{cm}^{-3}$, geometric standard deviation of 1·4 and mean particle diameter of 0·6 μm. The condensation coefficients a_i in equation (24) are equal to $10^{-10}\ \mathrm{g}^{2/3}\,\mathrm{s}^{-1}$. Figure 1 shows the numerical results at 10 s from the moving finite element method (MULFEMM), the Smolarkiewicz method and the upwind-differencing method. The ordinate and abcissa of the contour plots are the J-values for the two components. The diagrams on the left-hand side are top views of the size distribution while those on the right-hand side are 3D views from the south-east corner. The contour values on the left and the vertical scales on the right are logarithms of the number distribution function $f(J1, J2)$. The adjacent contour lines are 0·5 units apart. Contours with steep gradients (e.g. Figures 1(a) and 1(b) appear to be disconnected and incomplete. This is due to the limitations of the Surface-II plotting routine. It is obvious that the moving finite element method (MULFEMM) compares favourably with the analytical solution, whereas the Smolarkiewicz method and the upwind-differencing method suffer from intolerable numerical diffusion. Table I shows that the moving finite element method predicts the correct peak location and value of the size distribution. It also has the lowest value of the error function $\| E \|$. M_0 and M_1, the zeroth and first moments of the size distribution f, which correspond to the number and mass concentration of the particles, are close to the analytical solution. The number concentraions predicted by the Smolarkiewicz method and the upwind-differencing method are exact because the condensation process is number-conserving and both numerical schemes are number-conserving schemes. However, both methods predict incorrect size distributions. This pitfall points out that the use of moments of the size distribution as the only measure of accuracy is not sufficient.

Case 2. Fast growth process with equal condensation rates

The condensation coefficients are the same as those in case 1. However, the initial size distribution is characterized by the initial number concentration of $8{\cdot}823 \times 10^6\ \mathrm{cm}^{-3}$, geometric standard deviation of 1·5 and mean particle diameter of 0·1 μm. Because of its smaller mean

Table I. Comparison of different numerical schemes with analytical solution for case 1 at time level of 10 s. Condensation coefficients $a_1 = a_2 = 10^{-10}\ \mathrm{g}^{2/3}\,\mathrm{s}^{-1}$; initial mean diameter 0·6 μm

	Grid spacing ΔJ	Time step (s)	Peak location $J1$	$J2$	Peak value $\times 10^{-6}$	$\| E \| \times 10^2$	$M_0 \times 10^{-6}$ (cm^{-3})	$M_1 \times 10^7$ ($\mathrm{g\ cm}^{-3}$)
MULFEMM	0·3	0·1	19·702 ($0{\cdot}74\ \mu$m)	19·702	3·470	0·128	1·672	3·849
Smolarkiewicz	0·3	0·1	19·600 ($0{\cdot}72\ \mu$m)	19·600	2·212	8·388	1·670	3·828
Upwind differencing	0·3	0·1	19·600 ($0{\cdot}72\ \mu$m)	19·600	1·001	14·9	1·670	3·902
Analytical solution			19·702 ($0{\cdot}74\ \mu$m)	19·702	3·500		1·670	3·869

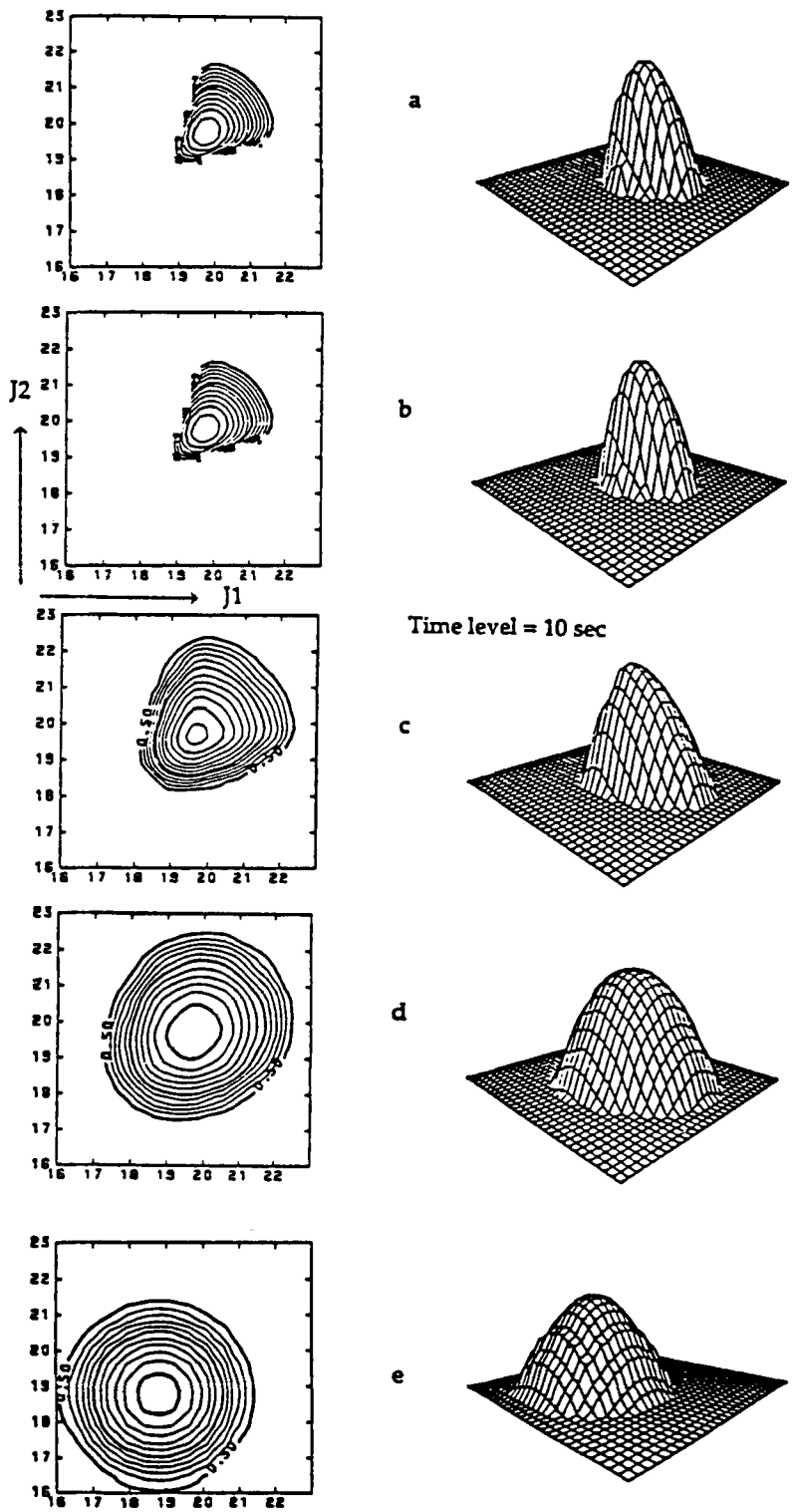

Figure 1. Comparison of (a) analytical solution, (b) MULFEMM, (c) Smolarkiewicz method and (d) upwind-differencing method for case 1, which is a slow growth process with equal condensation rates; (e) is the initial size distribution

diameter, there is a rapid change in size distribution. Figure 2 shows the evolution of the size distribution and the grid system from MULFEMM. The initial size distribution and the grid system with grid spacing of 0·5 are shown in the bottom figures. The initial grid system is 32×32 but the 3D plots on the right-hand side use 64×64 lines for better representation. As particles grow, the size distribution approaches monodispersity. At $t = 10$ s, particles are almost of the

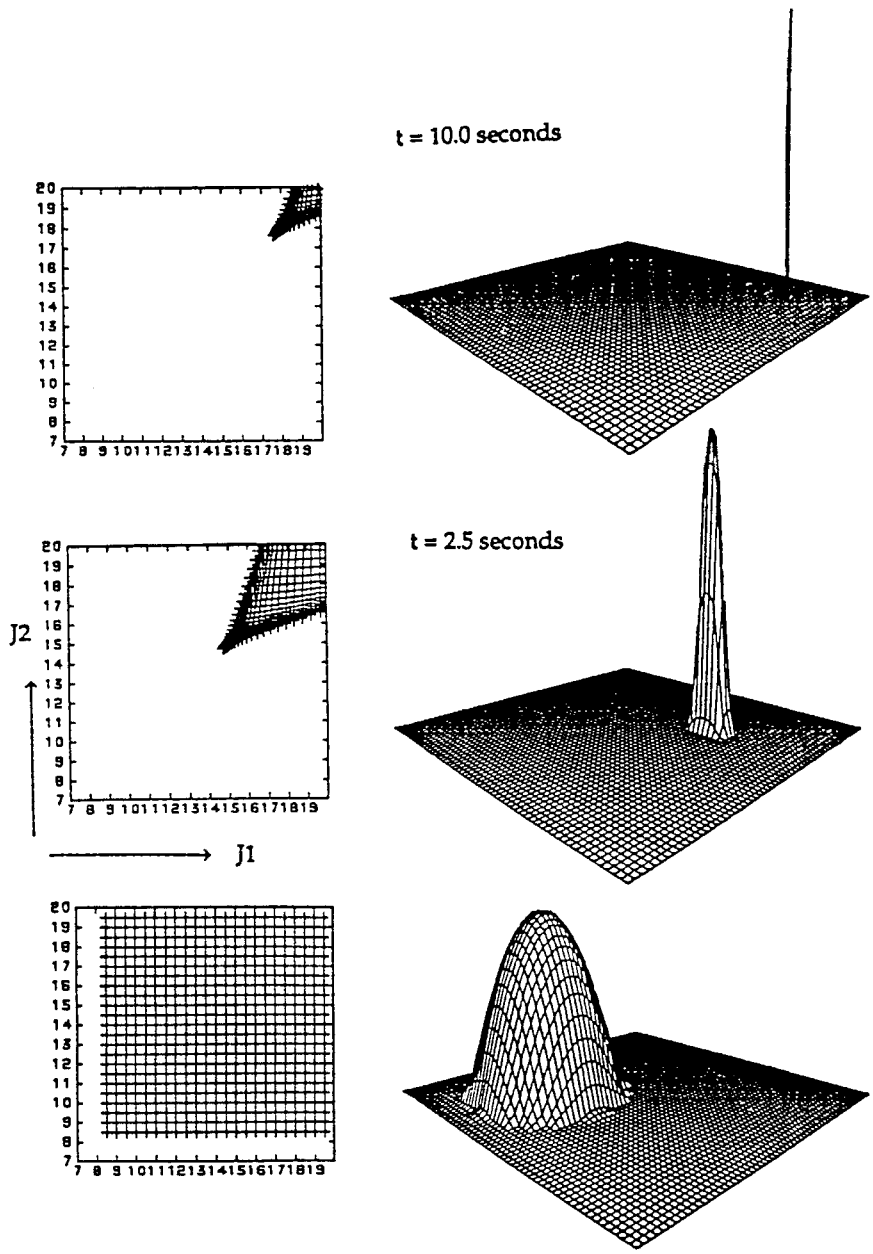

Figure 2. MULFEMM's numerical solution and grid movement at two time levels for case 2, which is a fast growth process with equal condensation rates; the initial size distribution and grid system are shown at the bottom.

same size and extremely large gradients exist around the narrow size distribution. Notice that the grids are moved to where high resolution is required. Figure 3 compares the numerical solutions by MULFEMM and the analytical solutions at $t=2{\cdot}5$ s and $t=10$ s by magnifying the region in close proximity to the solution. The grid spacing in the areas where the steepest gradients are encountered has $\Delta Ji=0{\cdot}005$. A fixed grid system with such grid spacing using the Smolarkiewicz method or the upwind-differencing method would need some 3000 grid points in each direction. Figure 4 shows that, even at $t=2{\cdot}5$ s, the Smolarkiewicz method and the upwind-differencing method create excessive numerical diffusion. Table II shows grid spacing, time step size and the results by the different methods at the time level of 2·5 s. The Courant number stability criterion for the Smolarkiewicz method and the upwind-differencing method requires a maximum time step of 0·003 s for the grid spacing of 0·5. The CPU times on an IBM 3090-300E computer for simulations up to the time level of 2·5 s are 2490 s for the upwind-differencing method, 3240 s for the Smolarkiewicz method and 1815 s for MULFEMM. The computational efficiency of MULFEMM is due to the fact that it can allow the use of a much larger time step. Another simulation using MULFEMM is conducted to illustrate its ability to use unequal grid spacing to improve

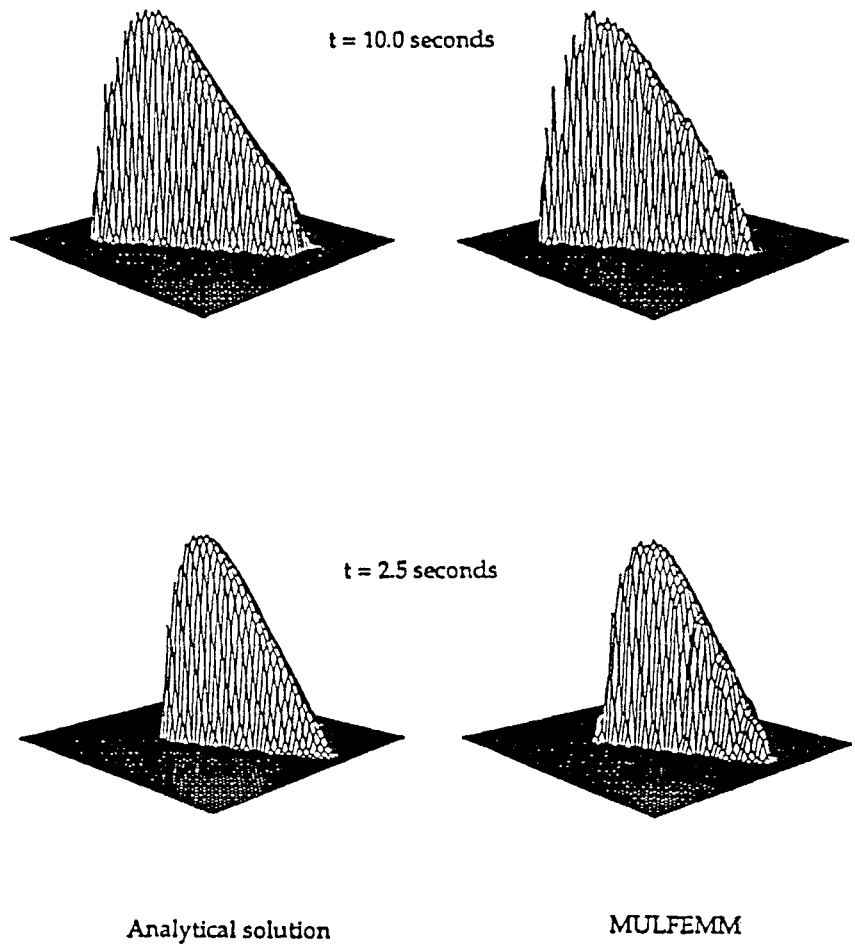

Figure 3. Comparison of MULFEMM's numerical solution with the analytical solution for case 2

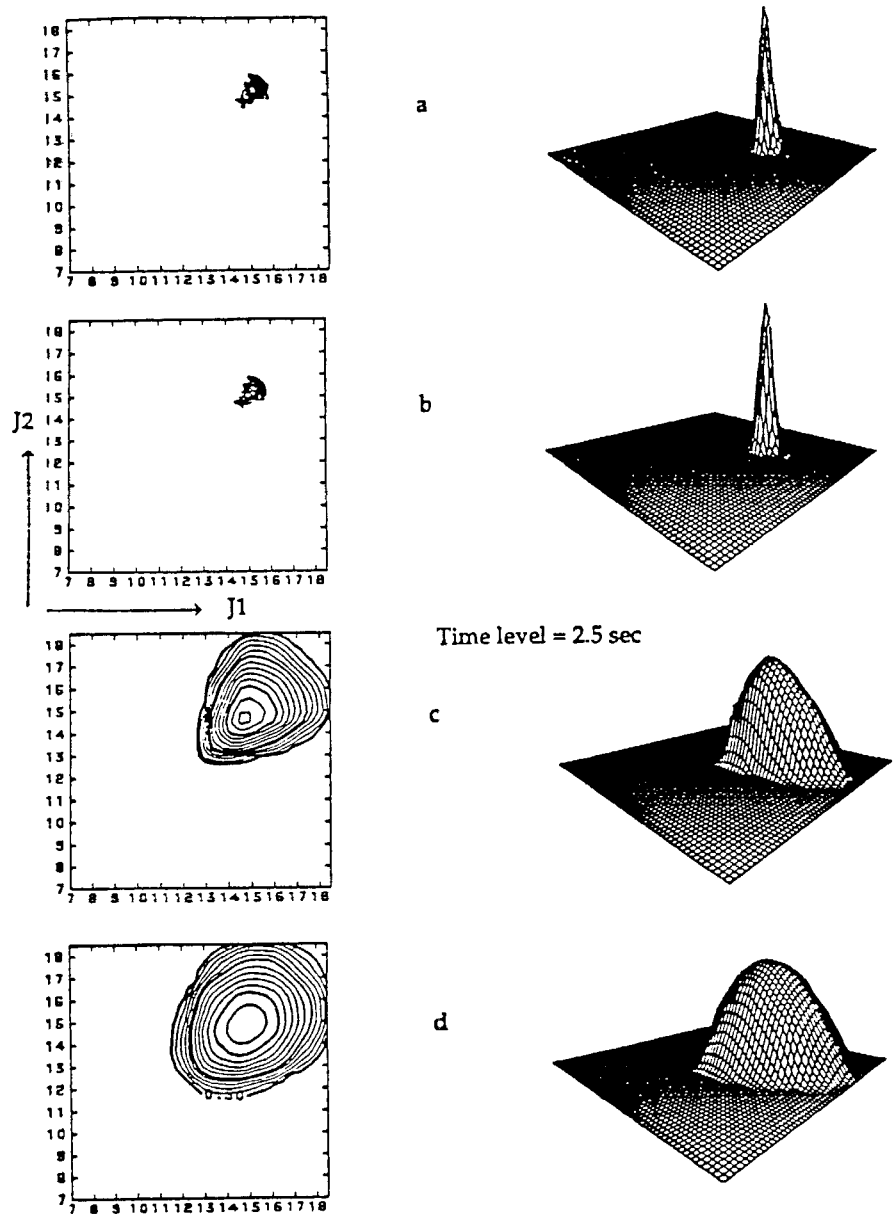

Figure 4. Comparison of (a) analytical solution, (b) MULFEMM, (c) Smolarkiewicz method and (d) upwind-differencing method for case 2 at 2.5 s

the result while retaining the same total number of grid points. Initially, a grid spacing of 0·25 is used to model the cone of the initial distribution while the grid spacing elsewhere is increased to 0·75. The improvement obtained in the solution is about 10% with regard to the peak value, and the error decreases by a factor of three (see case MULFEMM(b) in Table II).

Table II. Comparison of different numerical schemes with analytical solution for case 2 at time level of 2·5 s. Condensation coefficients $a_1 = a_2 = 10^{-10}\,g^{2/3}\,s^{-1}$; initial mean diameter 0·1 μm

	Grid spacing ΔJ	Time step (s)	Peak location $J1$	$J2$	Peak value $\times 10^{-6}$	$\|E\| \times 10^2$	$M_0 \times 10^{-6}$ (cm^{-3})	$M_1 \times 10^8$ ($g\,cm^{-3}$)
MULFEMM(a)	0·5	0·01	14·951 (0·247 μm)	14·951	319·5	3·45	7·726	6·171
MULFEMM(b)	0·25	0·01	14·913 (0·245 μm)	14·913	362·1	1·13	8·236	6·574
Smolarkiewicz	0·5	0·002	14·500 (0·223 μm)	14·500	6·3	14·51	8·823	6·786
Upwind differencing	0·5	0·002	15·000 (0·250 μm)	15·000	2·9	48·18	8·823	7·464
Analytical solution			14·913 (0·245 μm)	14·913	411·4		8·823	7·153

Table III. Comparison of different numerical schemes with analytical solution for case 3 at time level of 5 s. Condensation coefficients $a_1 = 10^{-14}\,g^{2/3}\,s^{-1}$, $a_2 = 10^{-10}\,g^{2/3}\,s^{-1}$; initial mean diameter 0·1 μm

	Grid spacing ΔJ	Time level (s)	Peak location $J1$	$J2$	Peak value $\times 10^{-5}$	$\|E\| \times 10^2$	$M_0 \times 10^{-6}$ (cm^{-3})	$M_1 \times 10^8$ ($g\,cm^{-3}$)
MULFEMM	0·25	0·02	11·004 (0·246 μm)	15·873	499·2	1·41	8·851	7·049
Smolarkiewicz	0·5	0·002	11·000 (0·253 μm)	15·500	49·4	23·29	8·823	6·828
Upwind differencing	0·5	0·002	11·000 (0·253 μm)	16·000	31·2	23·82	8·823	7·557
Analytical solution			11·004 (0·246 μm)	15·873	501·6		8·823	7·103

Case 3. Gowth process with unequal condensation rates

The initial size distribution is the same as that of case 2. However, the condensation efficients are four orders of magnitude different: $a_1 = 10^{-14}\,g^{2/3}\,s^{-1}$, $a_2 = 10^{-10}\,g^{2/3}\,s^{-1}$. The Courant number stability criterion is the same as that for case 2. Table III shows that MULFEMM, using a smaller initial grid spacing and ten times larger time step, produces excellent results. Figure 5 shows that as the growth process continues, the size distribution becoming a thin slice moving in the $J2$-direction, MULFEMM can reproduce the analytical solution very well whereas the Smolarkiewicz method and the upwind-differencing method still create a cone-shaped size distribution indicating excessive numerical diffusion. Table III shows that there is significant improvement in the peak value and the error function for the Smolarkiewicz and the upwind-differencing methods as compared with the results for equal condensation rates shown in Table II. This is due to the fact that case 3 is a growth process essentially dominated by the second component.

Case 4. Growth of dioctyl phthalate (DOP) and dibutyl phthalate (DBP) system

Having validated the moving finite element method (MULFEMM) with analytical solutions, we compare different numerical results for this realistic aerosol system for which no analytical

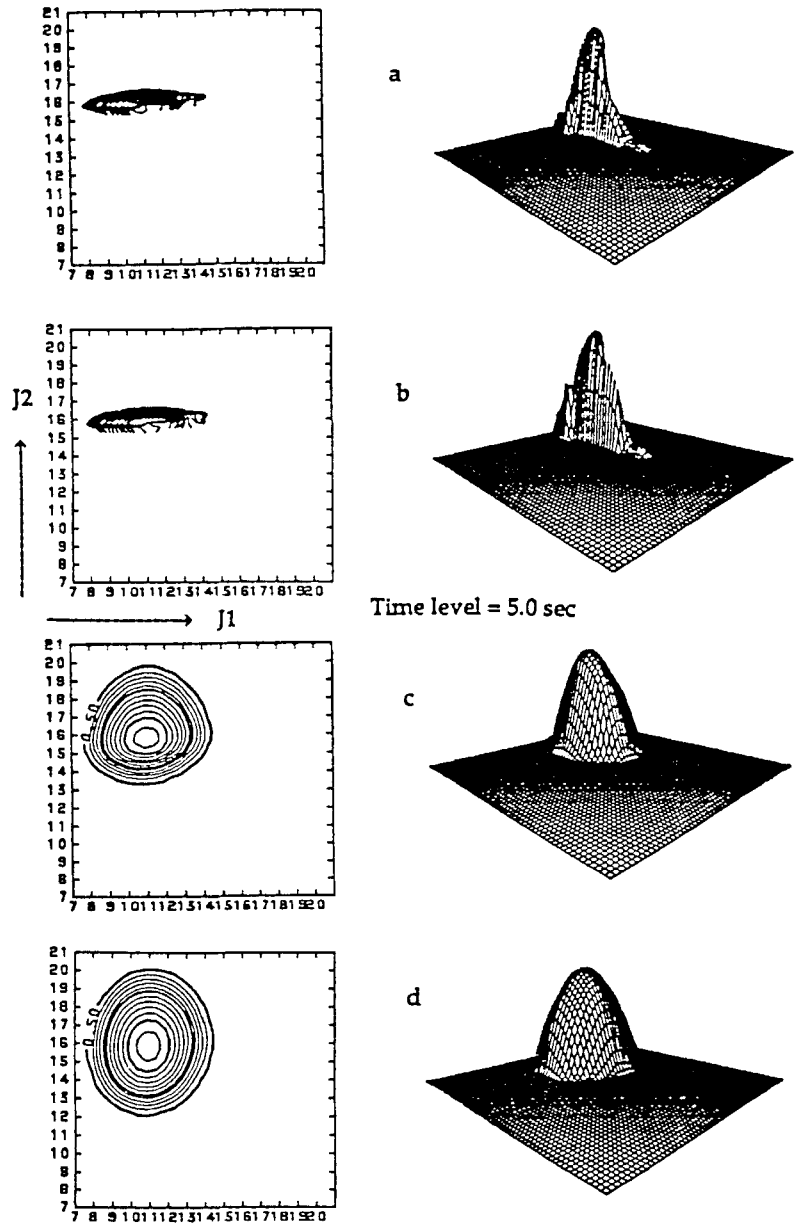

Figure 5. Comparison of (a) analytical solution, (b) MULFEMM, (c) Smolarkiewicz method and (d) upwind-differencing method for case 3, which is a fast growth process with four orders of magnitude difference in condensation rates

solution is available. The initial size distribution is the same as that of case 3. The mean free paths of DOP and DBP are assumed to be $6{\cdot}5 \times 10^{-6}$ cm. The surface tension of the solution droplet is 25 dyn cm^{-1}. The molecular weight and the vapour pressure of DOP and DBP are 390, 278 and 5×10^{-6}, 5×10^{-4} mmHg respectively. The 3D plots are viewed from the north-east corner. The system temperature is 50 °C and the saturation ratio of each component is maintained at 2·0. In this case study the Kelvin effect and the Fuchs interpolation (formula (i.e. equations (4) and (5))

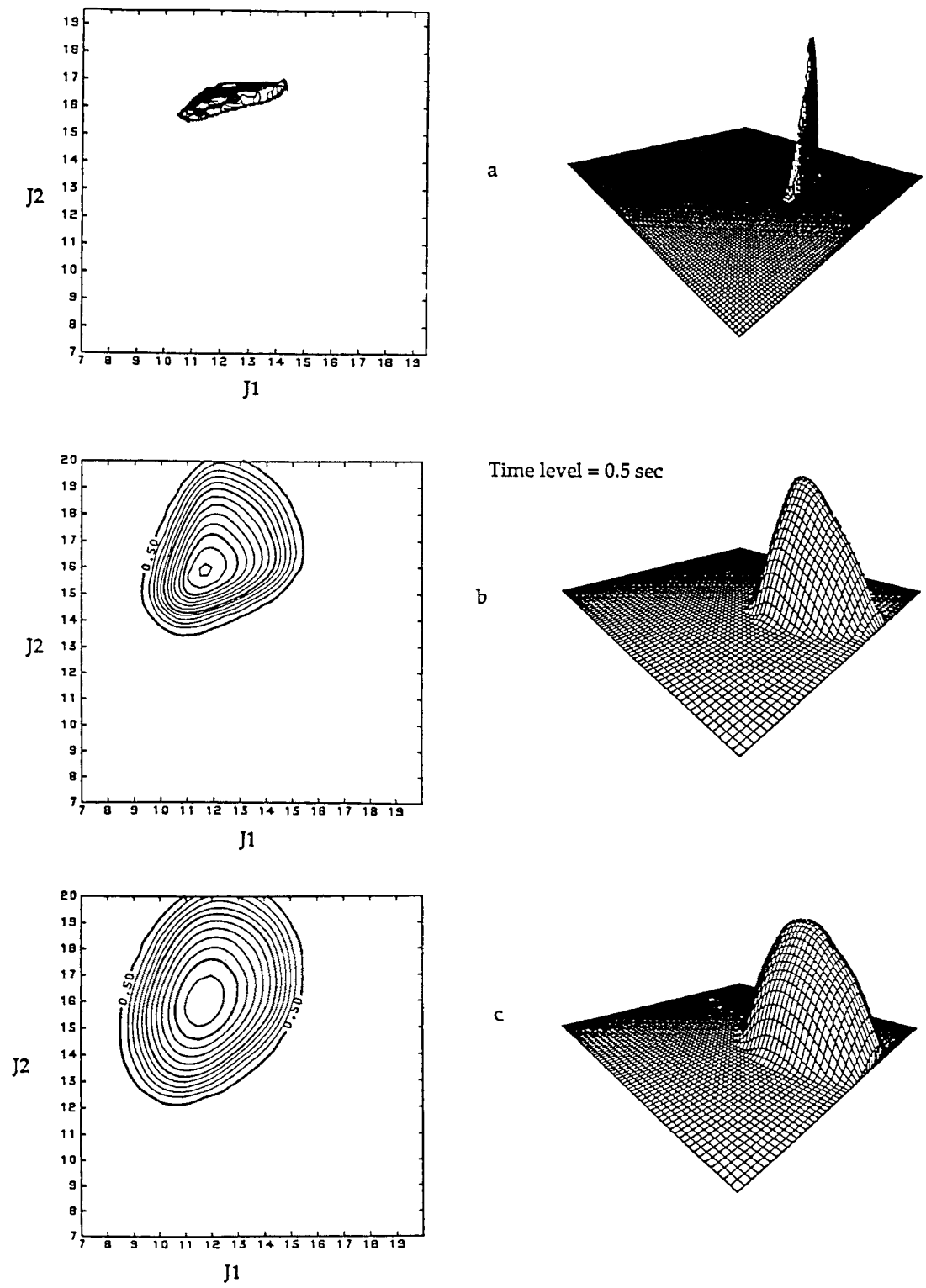

Figure 6. Comparison of (a) MULFEMM, (b) Smolarkiewicz method and (c) upwind-differencing method for case 4, the DOP/DBP system

are included. Figure 6 shows that MULFEMM provides reliable numerical result whereas the Smolarkiewicz and the upwind-differencing methods create intolerable numerical diffusion. The peak values of the size distribution are $7{\cdot}51 \times 10^7$, $5{\cdot}1 \times 10^6$ and $2{\cdot}7 \times 10^6$ for MULFEMM, Smolarkiewicz and upwind differencing respectively. Furthermore, there is a significant difference in size distribution, as expected. In these studies the latent heat released by condensation has not been included in the simulations. This is valid for DOP/DBP systems since the heat of vaporization and the mass transfer rates are very small. For volatile compounds, Tsang *et al.*[21] showed that the latent heat effect can be incorporated into the growth rate in equation (4). Furthermore, the generalized Stefan–Maxwell equation can be used instead of the Maxwell equation (2).

In the derivation of equation (17) we assumed that each element in the $J1$–$J2$ plane is treated as a rectangle rather than a quadrilateral. Case 2 represents the most severe test on the simplification of the Jacobian because the points are moved rapidly to the diagonal and the elements are much distorted from rectangles. For example, the first element in Figure 4(b) has the following ($J1$, $J2$) co-ordinates (14·6773, 14·6773), (14·6879, 14·6939), (14·6922, 14·6864) and (14·7019, 14·7019). Obviously, the element is much deviated from a rectangle. On the other hand, in case 3, where the condensation rate of the second component is 10 000 times higher than that of the first component, we expect the elements will remain closer to rectangular shape since the grid points move very slowly in the $J1$-direction. The co-ordinates of the first element in Figure 5(b) are as follows: (7·7837, 15·6410), (7.7838, 15·6467), (8.0285, 15·6455) and (8·0286, 15·6510). For case 2, even after the size distribution becomes practically monodisperse at 10 s, MULFEMM still provides satisfactory results. This implies that it is more important to locate the grid points to where they are needed most than to evaluate the Jacobian rigorously.

The banded matrix problem in equation (22) is solved by the MA28 sparse matrix code[22] in NAGLIB. We have also obtained excellent preliminary results for ternary systems. For case 2, MA28 requires arrays of $12pu + 15u$ elements, where p is the number of diagonals in equation (22) ($p = 5$ for binary systems) and u is the number of unknowns. Finally, it should be pointed out that the success of MULFEMM is due to the fact that the grids are moved to where high resolution is needed. In principle, finite difference schemes with moving grid methods may also be used to model these particle growth problems, as evidenced by the recent work of Thomaidis *et al.*[23] on one-dimensional convection-dominated diffusion problems. For large-scale problems, use of the incomplete block factorization method[24] is under way.

CONCLUSIONS

We have presented an extension to the multidimensional case of the moving finite element method for the one-dimensional time-dependent convective transport and particle growth problems introduced in References 11 and 12

The method can be used for multicomponent particle growth processes. We have restricted ourselves to binary systems, although we have obtained excellent preliminary results for ternary systems. Comparisons with the positive definite methods of Smolarkiewicz and upwind differencing show that the moving finite element method is a reliable numerical technique whch can provide accurate results for a wide range of particle growth parameters.

ACKNOWLEDGEMENT

This work is supported by the Center of Computational Sciences in the University of Kentucky.

REFERENCES

1. D. Ramakrishna, 'The status of population balances', *Rev. Chem. Eng.*, **3**, 49–95 (1985).
2. T. H. Tsang and J. R. Brock, 'Dispersion of a plume of volatile aerosol', *Aerosol Sci. Technol.*, **2**, 426–436 (1983).
3. J. R. Brock, 'On size distribution of atomospheric aerosols', *Atmos. Environ.*, **5**, 833–841 (1971).
4. P. Ravindran and E. J. Davis, 'Multicomponent evaporation of single aerosol droplets', *J. Colloid Interface Sci.*, **85**, 278–288 (1982).
5. P. Mirabel and H. Reiss, 'Resolution of the "Renninger–Wilemski problem" concerning the identification of heteromolecular nuclei', *Langmuir*, **3**, 228–234 (1987).
6. G. Wilemski, 'Some issues of thermodynamic consistency in binary nucleation theory', *J. Chem. Phys.*, **88**, 5134–5136 (1988).
7. G. M. Hidy and J. R. Brock, *The Dynamics of Aerocolloidal Systems*, Pergamon Press, Oxford, 1970.
8. N. A. Fuchs and A. G. Sutugin, 'High-dispersed aerosols', in G. M. Hidy and J. R. Brock (eds), *Topics in Current Aerosol Research*, Pergamon Press, Oxford, 1971, Chap. 1.
9. A. K. Ray, J. Lee and H. L. Tilley, 'Direct measurements of evaporation rates of single droplets at large Knudsen numbers', *Langmuir*, **4**, 631–637 (1988).
10. P. Middleton and J. R. Brock, 'Simulation of aerosol kinetics', *J. Colloid Interface Sci.*, **54**, 249–264 (1976).
11. T. H. Tsang and J. R. Brock, 'Simulations of condensation and evaporation of condensation aerosol', *Aerosol Sci. Technol.*, **2**, 311–320 (1983).
12. E. Varoglu and W. D. L. Finn, 'Finite elements incorporating characteristics for one-dimensional diffusion–convection equation', *J. Comput. Phys.*, **34**, 371–389 (1980).
13. R. Lohner, 'Finite elements in CFD: what lies ahead', *Int. j. numer. methods eng.*, **24**, 1741–1756 (1987).
14. P. Devloo, J. T. Oden and T. Strouboulis, 'Implementation of an adaptive refinement technique for the SUPG algorithm', *Comput. Methods Appl. Mech. Eng.*, **61**, 339–358 (1987).
15. J. T. Oden, T. Strouboulis and P. Devloo, 'Adaptive finite element methods for high-speed compressible flows', *Int. j. numer. methods fluids*, **7**, 1211–1228 (1987).
16. J. G. Blom, J. M. Sanz-Serna and J. G. Verwer, 'On simple moving grid methods for one-dimensional evolutionary partial differential equations', *J. Comput. Physics*, **74**, 191–213 (1988).
17. T. H. Tsang and A. Rao, 'Comparison of different numerical schemes for condensational growth of aerosols', *Aerosol Sci. Technol.*, **9**, 271–277 (1988).
18. P. K. Smolarkiewicz, 'A fully-multidimensional positive definite algorithm with small implicit diffusion', *J. Comput. Phys.*, **54**, 325–362 (1984).
19. O. B. Toon, R. P. Turco, D. Westphal, R. Malone and M. S. Liu, 'A multidimensional model for aerosols: description of computational analogs', *J. Atmos. Sci.*, **45**, 2123–2143 (1988).
20. A. I. Flossmann, W. D. Hall and H. R. Pruppacher, 'A theoretical study of the wet removal of atmospheric pollutants. Part I: The redistribution of aerosol particles captured through nucleation and impaction scavenging by growing cloud drops', *J. Atmos. Sci.*, **42**, 583–606 (1985).
21. T. H. Tsang, S. M. Cook and M. E. Marra, 'The dynamic behavior of condensation and evaporation of polydisperse volatile aerosols', *Aerosol Sci. Technol.* in the press.
22. I. S. Duff and J. K. Reid, 'Some design features of a sparse matrix code', *ACM Trans. Math. Software*, **5**, 18–35 (1979).
23. G. Thomaidis, K. Zygourakis and M. F. Wheeler, 'An explicit finite difference scheme based on the modified method of characteristics for solving convection–diffusion problems in one-space dimension', *Numer. Methods PDE*, **4**, 119–138 (1988).
24. O. Axelsson, 'Incomplete block matrix factorization preconditioning methods. The ultimate answer?', *J. Comput. Appl. Math.*, **12/13**, 3–18 (1985).